AGU PUBLICATIONS

JGR

Journal of Geophysical Research: Atmospheres

RESEARCH ARTICLE
10.1002/2014JD022371

Key Points:
- Presents the midlatitude and subtropical ozone trends
- Shows clear recovery signal in the upper stratosphere
- Lower stratospheric recovery is now masked by the dynamics

Correspondence to:
P. J. Nair,
pjnnair@yahoo.in

Citation:
Nair, P. J., et al. (2015), Subtropical and midlatitude ozone trends in the stratosphere: Implications for recovery, *J. Geophys. Res. Atmos.*, *120*, 7247–7257, doi:10.1002/2014JD022371.

Received 2 AUG 2014
Accepted 1 JUN 2015
Accepted article online 5 JUN 2015
Published online 31 JUL 2015

Subtropical and midlatitude ozone trends in the stratosphere: Implications for recovery

P. J. Nair[1], L. Froidevaux[2], J. Kuttippurath[3], J. M. Zawodny[4], J. M. Russell III[5], W. Steinbrecht[6], H. Claude[6], T. Leblanc[7], J. A. E. van Gijsel[8], B. Johnson[9], D. P. J. Swart[10], A. Thomas[11], R. Querel[11], R. Wang[12], and J. Anderson[5]

[1]Centre for Earth Science Studies, Thiruvananthapuram, India, [2]Jet Propulsion Laboratory, California Institute of Technology, Pasadena, California, USA, [3]Indian Institute of Technology Kharagpur, West Bengal, India, [4]NASA Langley Research Center, Hampton, Virginia, USA, [5]Hampton University, Hampton, Virginia, USA, [6]Deutscher Wetterdienst, Hohenpeißenberg, Germany, [7]Jet Propulsion Laboratory, California Institute of Technology, Wrightwood, California, USA, [8]Royal Netherlands Meteorological Institute, De Bilt, Netherlands, [9]National Oceanic and Atmospheric Administration, Boulder, Colorado, USA, [10]National Institute for Public Health and the Environment, Bilthoven, Netherlands, [11]National Institute of Water and Atmospheric Research, Lauder, New Zealand, [12]Georgia Institute of Technology, Atlanta, Georgia, USA

Abstract We present a comprehensive analysis of the trends of stratospheric ozone in the midlatitudes and subtropics. The analysis is performed using ground-based and space-based measurements over the light detection and ranging stations for the period 1985–2012. Also, trends are estimated for the zonal mean data made from a merged satellite data set, Global OZone Chemistry And Related trace gas Data records for the Stratosphere, over 1979–2012. The linear trends in stratospheric ozone are estimated using piecewise linear trend (PWLT) functions. The ozone trends during the increasing phase of halogens (before 1997) range from -0.2 ± 0.08 to $-1\pm0.07\%$ yr^{-1} in the midlatitudes and -0.2 ± 0.06 to -0.7 ± 0.05 % yr^{-1} in the subtropics at 15–45 km, depending on altitude. In 1997–2012, the PWLT analyses show a positive trend, significantly different from zero at the 95% confidence intervals, toward ozone recovery in the middle- and low-latitude upper stratosphere (35–45 km), and the trends are about $+0.5\pm0.07\%$ yr^{-1} at midlatitudes and about $+0.3\pm0.05\%$ yr^{-1} at subtropical latitudes. However, negative and insignificant trends are estimated in the lower stratosphere (15–20 km) over 1997–2012 in the midlatitudes, mainly due to the dynamics, as demonstrated by the large (50–60%) contributions from the quasi-biennial oscillation, El Niño–Southern Oscillation, and planetary wave activity to recent ozone changes. This suggests that the ozone changes are governed by the interannual variations in meteorology and dynamics of the regions; these factors will influence the recovery detection time and the behavior of the recovery path to pre-1980 levels.

1. Introduction

Significant reduction in ozone has been observed in the midlatitudes due to the high levels of halogen compounds in the atmosphere since the 1980s [*World Meteorological Organization* (*WMO*), 2011]. Analysis using various satellite- and ground-based ozone data reveals that the upper stratospheric trends are about −6 to −8% decade^{-1} in the midlatitudes and −4.5% decade^{-1} in the subtropics before 1997 [*Steinbrecht et al.*, 2006]. Since the inception of the Montreal Protocol in 1987, noticeable decreases in the midlatitude halogen levels have been observed and this is reflected in the ozone trends there too [*WMO*, 2011]. Climate model simulations predict the total column ozone recovery to pre-1980 levels, associated with the reduction in stratospheric halogens, by around 2050 [*WMO*, 2011]. Recent studies expose a statistically significant positive trend toward ozone recovery in the northern midlatitudes from the observations over the period 1997–2010 [*Steinbrecht et al.*, 2011; *WMO*, 2011; *Nair et al.*, 2013; *WMO*, 2014]. Therefore, in this study, we make a comprehensive analysis of the trends in stratospheric ozone in the midlatitudes and subtropics using high-resolution ground-based measurements complemented by space-based measurements.

Multiple linear regression analysis with respect to the most important drivers of ozone variations, namely, quasi-biennial oscillation (QBO), solar flux (SF), aerosol optical thickness, heat flux (HFx), and El Niño–Southern Oscillation (ENSO) as well as the decadal trend terms, is applied for tracking changes in ozone. Our analysis is based on the ground-based and satellite measurements at various Network for the Detection of

Atmospheric Composition Change (NDACC) light detection and ranging (lidar) stations and using zonal mean data from GOZCARDS (Global OZone Chemistry And Related trace gas Data records for the Stratosphere) in the midlatitudes and subtropics.

This article is organized with the description of data sets in section 2 and the regression method in section 3. The evolution of ozone and trend estimates are presented in section 4 and the concluding remarks in section 5.

2. Data and Methods

The lidars use the differential absorption technique with an ozone absorption wavelength at 308 nm and a nonabsorption wavelength at either 355 nm or 353 nm. The lidar measurements from the Meteorological Observatory Hohenpeißenberg (MOHp: 48°N, 11°E), Tsukuba (36°N, 140°E), Jet Propulsion Laboratory-Table Mountain Facility (JPL-TMF: 34°N, 117°W), Mauna Loa Observatory (MLO: 19°N, 155°W), and Lauder (45°S, 169°E) during the periods 1987–2012, 1988–2010, 1988–2012, 1993–2012, and 1994–2012, respectively, are considered. Similarly, ozone observations carried out by the Brewer-Mast sondes at MOHp over 1987–2012, the Japanese KC sondes at Tateno over 1988–2009, and the ECC sondes at Hilo over 1991–2010 and Lauder over 1986–2012 are used. The ozonesonde data for Tsukuba and MLO are taken from their nearest soundings at Tateno (36°N, 140°E) and Hilo (19°N, 155°W), respectively.

Stratospheric Aerosol and Gas Experiment (SAGE) II on the Earth Radiation Budget Satellite (ERBS) uses the solar occultation technique. The version (v) 7.0 ozone number density profiles versus geometric altitudes from 1985 to 2005 are used [*Damadeo et al.*, 2013]. Halogen Occultation Experiment (HALOE) on the Upper Atmosphere Research Satellite (UARS) also uses solar occultation [*Russell et al.*, 1993], and v19 ozone volume mixing ratio (VMR) profiles for 1991–2005 are analyzed. Microwave Limb Sounder (MLS) on the Aura satellite measures thermal emission from the rotational lines of trace gases through the Earth's atmospheric limb. Aura MLS v3.3 ozone VMRs, retrieved from the 240 GHz radiometer data from 2004 to 2012 and screened as recommended by *Livesey et al.* [2011], are used here.

To estimate the trends in ozone, a stable and long-term ozone data set is made from lidar, ozonesondes, and satellite measurements with respect to the lidar stations, as described in detail by *Nair et al.* [2013]. The space-based measurements are extracted over the sites within ±5° latitude and ±10° longitude bands for SAGE II and HALOE and ±2.5° latitude and ±5° longitude bands for Aura MLS. All profiles extracted within this spatial domain are used for the analysis. The relative differences are estimated as [(meas-lidar)/lidar] × 100, where *meas* refers to the other instruments (e.g., ozonesondes, SAGE II, HALOE, and Aura MLS). The drift between the individual measurements is calculated from the slope of the monthly averaged relative difference time series by applying a simple linear regression. All measurements show their best agreement with respect to individual lidar measurements at 20–40 km, where the relative differences are ±5% and the individual data drifts are within ±0.5% yr^{-1}. In general, the comparisons between lidars and SAGE II and lidars and HALOE show drifts of about ±0.3 to ±0.4%yr^{-1}. The drifts derived from the combined time series over the lidar stations are insignificant and are of the order of ±0.2% yr^{-1} at 20–40 km [e.g., *Nair et al.*, 2012], indicating the importance of creating merged data sets, to reduce the individual data biases and instrumental drifts in short-term data sets, to produce quality long-term data for meaningful trend studies [e.g., *Nair et al.*, 2013; *Jones et al.*, 2009; *Kyrölä et al.*, 2013; *Steinbrecht et al.*, 2011].

The GOZCARDS date record is made up of debiased monthly zonal averages from various satellite measurements [*Wang et al.*, 2013]. This data record is available as VMR on a pressure grid (25 levels from 1000 to 0.1 hPa) in 10° latitude bins [*Froidevaux et al.*, 2015]. The GOZCARDS merged ozone data v1.01 is adjusted to SAGE II average values, and its variations are derived from a combination of SAGE I v5.9_rev, SAGE II v6.2, HALOE v19, and UARS MLS v5 before November 2005, after which the variations follow the combination of Aura MLS v2.2 and Atmospheric Chemistry Experiment Fourier transform spectrometer v2.2 data.

3. Regression Analysis

In order to find trends in ozone over the sites, we use the approach used by *Nair et al.* [2013]. The number density profiles on geometric altitude levels are used for the regression analysis. Therefore, HALOE and Aura MLS ozone VMRs and ozonesonde measurements in partial pressure over each station are converted to number density using the meteorological data provided in the respective data files. The ozone anomaly in percent is calculated, as the ratio of the deseasonalized ozone (monthly mean ozone − monthly climatology) and the

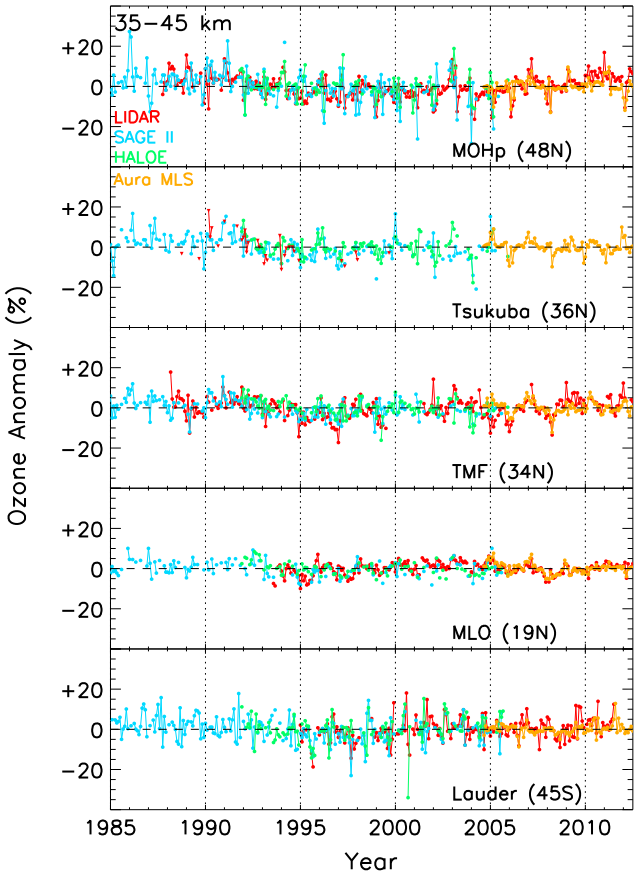

Figure 1. Temporal evolution of the ozone anomalies computed in the upper stratosphere (at 35–45 km) from different measurements used for ozone trend analysis over the lidar sites. According to the standard screening criterion (see text for details), the Tsukuba lidar ozone anomalies are not available in this altitude range. Therefore, the lidar ozone anomalies computed at 35–40 km with respect to the standard screening criterion are shown at Tsukuba.

monthly climatology, on a 1 km vertical grid. Figure 1 shows the anomalies computed from the ozone averaged over the 35–45 km altitude band for different data sets at each station. The anomaly at each station and instrument is calculated if there are at least two measurements in a month for each altitude and if the measurements are available for the whole altitude band. However, the Tsukuba lidar system often does not cover the altitudes above 30 km and typically reaches the end of its usable measurement range between 35 and 40 km, especially after 2000 [see also *Nair et al.*, 2012]. Therefore, the lidar ozone anomaly at 35–45 km cannot be obtained for Tsukuba, when the standard screening criterion is applied as for other stations. Hence, the lidar ozone anomalies computed for the 35–40 km altitude band are shown at Tsukuba. Tsukuba, therefore, makes a clear case for our decision to use the multi-instrument average ozone anomaly in our regression analysis (see the method description below).

The anomalies from each instrument at Lauder show values of around +5% in 1985–1992, a decrease of about −2 to −5% in 1993–2000, near-zero values in 2000–2010, and a very small increase thereafter [e.g., *WMO*, 2011]. A similar pattern of anomaly is also observed at all northern midlatitude stations (MOHp, Tsukuba, and TMF), but the negative anomaly in the mid-1990s is more pronounced at the northernmost lidar station MOHp [e.g., *Steinbrecht et al.*, 2009]. However, the anomalies computed for some years are comparatively larger (up to ±20% in some cases) as in the case of 2000 at Lauder and 2004 at MOHp. It has to be kept in mind that, from mid-1993 to mid-1994, there was a power problem on the ERBS that resulted in the complete loss of SAGE II sunset measurements during the period. This makes the monthly zonal means computed from the SAGE II measurements biased low in the upper stratosphere and thus a step-like feature in the anomaly at the subtropical stations (e.g., at MLO) where the diurnal effects are more prominent [*Damadeo et al.*, 2014]. Since the trends are derived using the average ozone anomaly computed from various satellite- and ground-based measurements, the estimated trends are less affected by the aforesaid problem. However, this can have a small impact on the ozone trends found from SAGE II data presented in section 4.3. The time evolution and magnitude of the ozone anomalies are very similar to those computed by *Steinbrecht et al.* [2006], *Nair et al.* [2013], and *Kirgis et al.* [2013] for the midlatitude lidar stations and *Jones et al.* [2009] at midlatitudes. Further discussion of the ozone anomalies is given in section 4.

The anomalies from different instruments are averaged to obtain a single data set at each site. The regression is performed on the average anomaly time series on a monthly basis. Note that a long-term stable data set is a prerequisite for the estimation of ozone trends. As emphasized above, the estimated drifts from relative differences between the combined ozone data and ozone lidar data are insignificant and smaller than those between the individual data sets. This implies that the combination leads to a less noisy long-term data set suitable for the evaluation of ozone trends. Moreover, this combined and consolidated data set makes use of

comparatively short-term data sets to obtain reliable trend estimates [e.g., *Nair et al.*, 2013; *Jones et al.*, 2009; *Steinbrecht et al.*, 2009]. The regression model used for computing ozone trends is

$$\begin{aligned} O_3(n) = & K + R_1 t1(n) + R_2 t2(n) + R_3 \text{Aerosol}(n) + R_4 \text{HeatFlux}(n) \\ & + R_5 \text{SolarFlux}(n) + R_6 \text{ENSO}(n) \\ & + R_7 \text{QBO10hPa}(n) + R_8 \text{QBO30hPa}(n) + e(n) \end{aligned} \quad (1)$$

where n is the running month, K is a constant, and e is the residual. The term $t1(n)$ is $n/12$ and $t2(n)$ is set to zero before the Effective Equivalent Stratospheric Chlorine (EESC) peak year and $(n-n_0)/12$ after the EESC peak year where n_0 is the running month corresponding to the previous year of the turnaround year. R_1 to R_8 are the coefficients of the respective proxies. Further details of the model can be found in *Reinsel et al.* [2002]. The regression is done for each calendar month (January to December) separately. The two linear ozone trends are estimated using time as a proxy and are considered as piecewise linear trends (PWLTs) with a turnaround year of 1997 for the midlatitudes and 1995 for the subtropics in conjunction with the year of the EESC maximum in the respective regions [*Newman et al.*, 2007]. The error of the regression coefficients is calculated using the generalized least squares method and by considering autocorrelation of residuals with a 1 year lag [*Press et al.*, 1989].

The deseasonalized aerosol optical thickness and heat flux data and the monthly data for other proxies are applied in the regression analysis. The specifications of the proxies used in the regression analysis are QBO indices at 10 and 30 hPa (http://www.geo.fu-berlin.de/en/met/ag/strat/produkte/), SF at 10.7 cm wavelength (ftp://ftp.ngdc.noaa.gov/STP/space-weather/solar-data/solar-features/solar-radio/noontime-flux/), aerosol optical thickness at 550 nm (http://data.giss.nasa.gov/modelforce/strataer/), ENSO (www.ncdc.noaa.gov/teleconnections/enso/), and HFx calculated from the ERA-Interim meteorological data at 100 hPa [*Kuttippurath and Nikulin*, 2012] averaged over 45–75°N for the northern midlatitudes and 45–75°S for the southern midlatitudes [*Kuttippurath et al.*, 2013], and 45–75°N during November to April and 45–75°S during May to October for the subtropics, as done by *Wohltmann et al.* [2007]. The correlation between ozone production and accumulation of HFx during winter is also taken into account [*Wohltmann et al.*, 2007].

4. Results and Discussions

Figure 2 shows the temporal evolution of the vertical distribution of average ozone anomaly and regressed output for various stations over 1985–2012. A 5 month smoothing is applied to the data as it increases the correlation between the ozone anomaly and regressed output because smoothing reduces the discontinuity of the time series and suppresses undesired peaks. To avoid the effect of a relatively higher tropopause in the subtropics, results are not shown below 20 km at MLO. As shown in the figure, in general, at all stations, relatively large positive anomalies are found at the beginning of the period, negative in 1995–1997, and slightly positive (see also the later analyses) at the end of the 2000s, in concert with the abundances of halogens in the stratosphere during each period [e.g., *WMO*, 2011; *Jones et al.*, 2009]. In general, the coefficient of multiple determination (R^2) is calculated to be about 60–85%, showing that the regressed data explain much of the observed ozone variability in both hemispheres above 20 km at all stations. In addition, most of the anomalies are within ±5%, indicating a very good agreement between the regressed data and measurements [e.g., *Nair et al.*, 2013; *Kirgis et al.*, 2013; *Steinbrecht et al.*, 2009].

The regressed output also clearly replicates the high ozone in the lower stratosphere in 2009 and 2010 at MOHp, primarily due to dynamical processes such as enhanced planetary wave activity in the easterly phase of QBO at northern midlatitudes, as mentioned previously [e.g., *Steinbrecht et al.*, 2011]. In contrast to 2010, 2011 and 2012 show negative ozone anomalies at MOHp, Tsukuba, and TMF, mainly in the lower stratosphere. During 2011 and 2012, descending westerlies in the tropical lower stratosphere resulted in suppressed residual circulation and hence less transport of ozone from the low to middle and high latitudes [*Long and Christy*, 2012]. The ENSO values also indicate that La Niña, capable of reducing ozone transport, was strengthened by 2011 and lasted up to mid-2012. These dynamical features could be the main reason for the low ozone amount at the northern midlatitude stations in 2011 and 2012.

To facilitate the connection between ozone anomaly and regressed output in Figure 2, the contribution of various proxies to the ozone change in the upper stratosphere (at 35–45 km) is given in Figure 3. The contribution of QBO to ozone is shown by adding the contributions of QBO at 10 and 30 hPa to ozone. All stations show

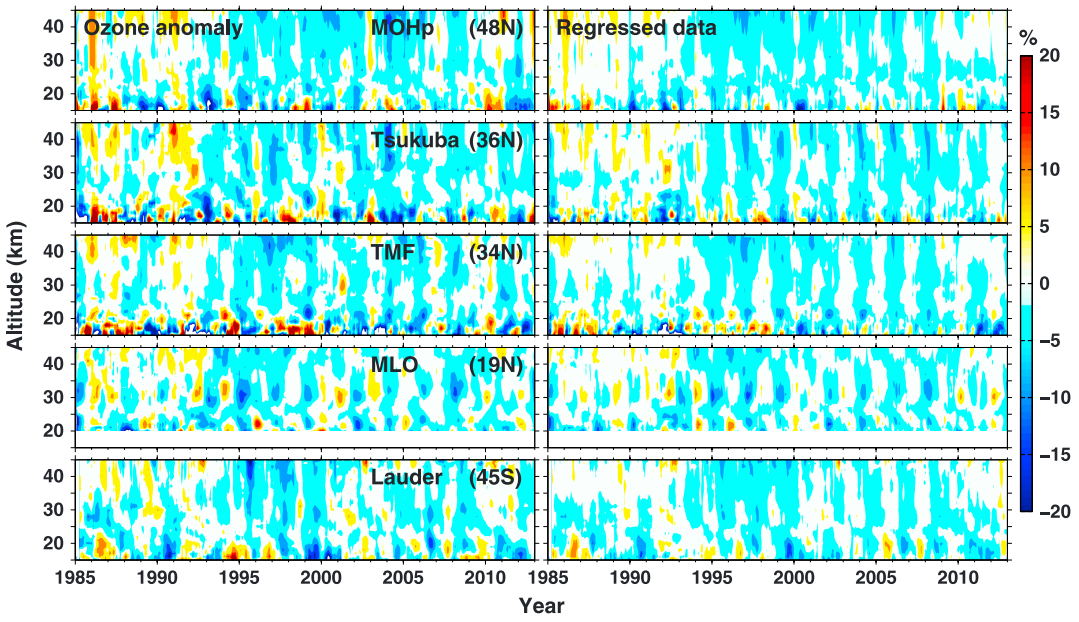

Figure 2. Temporal evolution of the vertical distribution of average ozone anomalies computed from lidar, ozonesondes, SAGE II, HALOE, and Aura MLS and the regressed output at various lidar sites over 1985–2012. At MLO, regression results are not shown below 20 km because of the higher tropopause there.

largest positive anomalies (3–8%) during 1985–1992, as the ozone decrease was in its initial phase in that period. The ozone decrease in the mid-1990s and the ozone increase in the late 2000s are more pronounced at the southernmost and northernmost latitude stations (Lauder and MOHp, respectively). In general, the ozone changes at the northern stations are comparatively dominated by the QBO, with changes within ±4%. The maximum contribution of aerosol to ozone is found during 1992, although there are differences in the peak amplitudes at different stations. This difference could be due to the influence of other proxies on ozone, as we perform a multilinear regression on a monthly basis. The planetary wave activity and thus the stratospheric circulation also play a key role in the ozone distribution at MOHp and Tsukuba, with peak-to-peak values of about −2 to +2%. As expected, the ozone changes are largely governed by the QBO at the subtropical station MLO. At MOHp and Tsukuba, the lowest ozone anomalies in the upper stratosphere are found in 2004, about −9%, and are contributed by the QBO at MOHp and QBO coupled with the wave activity at Tsukuba. The model fully explains the observed ozone anomaly in 2006 and 2007 at the northern midlatitude stations and is mainly contributed by the QBO. Also, the QBO explains the lowest ozone anomaly (−7%) observed at TMF in 1996. A large part of the positive anomaly (5%) at TMF and MLO in 1998 is driven by the ENSO, but the QBO induces a part of the largest negative anomaly in 1996 and the positive anomaly in 2011 at Lauder.

4.1. Trends During 1985–1997

Figure 4 (solid line) displays vertical profiles of trend estimates based on the analyses of average ozone anomalies over the lidar sites for the 1985–1997 (1985–1995 for MLO) period. At Lauder, the trends are of the order of -0.2 ± 0.05 to $-0.4 \pm 0.09\%\ yr^{-1}$ at 15–23 km and -0.5 ± 0.08 to $-0.8 \pm 0.07\% yr^{-1}$ at 31–45 km. At MLO, the trends range from $-0.2 \pm 0.06\%\ yr^{-1}$ at 26 km to $-0.7 \pm 0.08\%\ yr^{-1}$ at 45 km, whereas significant positive trends of about $+0.5 \pm 0.15\%\ yr^{-1}$ are found at 20–21 km. At TMF, the trends are around $-0.25 \pm 0.15\%\ yr^{-1}$ at 20–24 km, $-0.2 \pm 0.07\%\ yr^{-1}$ at 25–35 km, and -0.3 ± 0.07 to $-1 \pm 0.07\%\ yr^{-1}$ at 35–45 km. At Tsukuba, the trends are -0.2 ± 0.08 to $-0.4 \pm 0.07\%\ yr^{-1}$ at 18–24 km and around $-0.4 \pm 0.06\%\ yr^{-1}$ at 31–45 km. At MOHp, the estimated trends are -0.3 ± 0.1 to $-0.5 \pm 0.07\%\ yr^{-1}$ at 18–30 km and -0.6 ± 0.08 to $-1.0 \pm 0.07\%\ yr^{-1}$ at 31–45 km. In general, the largest negative trends of about -0.7 ± 0.08 to $-1 \pm 0.07\%\ yr^{-1}$ are observed at 35–45 km at all stations. Below 20 km, trends are less than $-0.5 \pm 0.10\%\ yr^{-1}$ (no data are shown for MLO in this region due to the higher tropopause there). The estimated trends are significantly different from zero at the 95% confidence intervals at all altitudes at MOHp, and above 30 km at other sites, while they are not significant over 16–17 km and 27–29 km at Tsukuba, 16–18 km at TMF, and 15 km and 22–25 km at Lauder. These results show a strong ozone decrease in the upper stratosphere and negligible trends in the middle stratosphere.

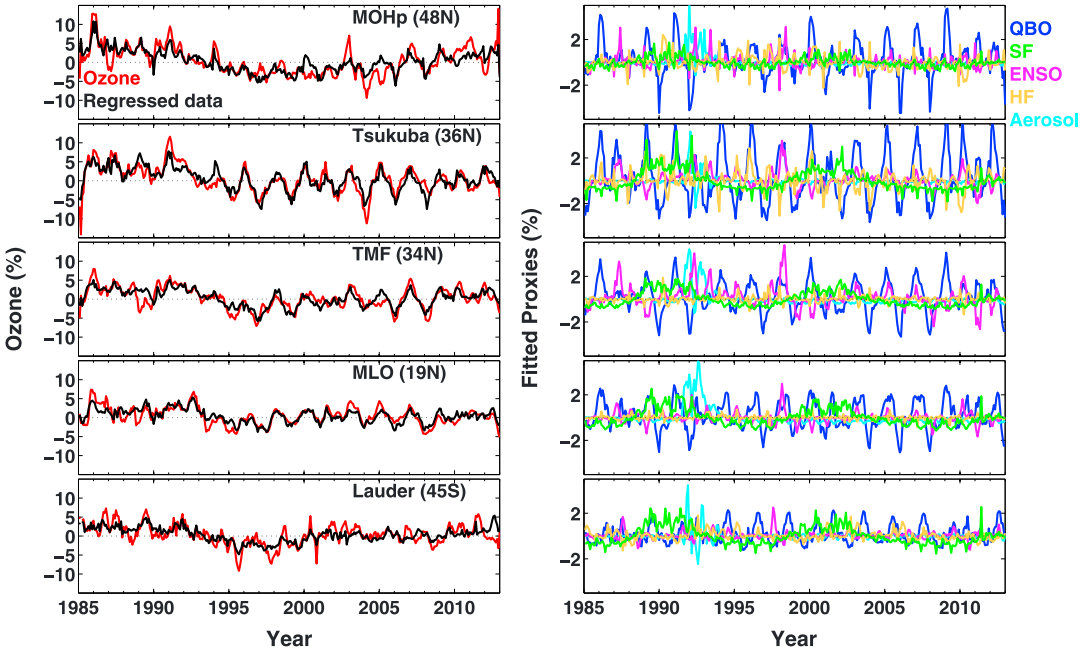

Figure 3. (left column) The ozone anomaly and regressed output over different sites in the upper stratosphere (at 35–45 km). (right column) The contribution of various proxies to the ozone change during 1985–2012.

On average, our estimates for the northern midlatitudes (derived from the average ozone anomaly over the stations MOHp, Tsukuba, and TMF) show $-0.3 \pm 0.07\%$ yr^{-1}, $-0.35 \pm 0.06\%$ yr^{-1}, and $-0.7 \pm 0.06\%$ yr^{-1} at 20–25 km, 25–35 km, and 35–45 km, respectively. These estimates are in good agreement with those estimated at northern midlatitudes (30–60°N) from satellite measurements in 1979–1997 by *Jones et al.* [2009], as they also find statistically significant trends of about $-0.38 \pm 0.08\%$ yr^{-1} at 20–25 km, $-0.33 \pm 0.07\%$ yr^{-1} at 25–35 km, and $-0.72 \pm 0.09\%$ yr^{-1} at 35–45 km. Similarly, our estimates are comparable to those evaluated from the combined SAGE II and Global Ozone Monitoring by Occultation of Stars (GOMOS) data for the northern midlatitudes in 1984–1997 (e.g., -0.7% yr^{-1} at 35–45 km) by *Kyrölä et al.* [2013], as listed in Table 1 (extracted from their Figure 14). Our upper stratospheric estimate is also in accordance with that found from satellite measurements by *Cunnold et al.* [2004] and *Wang et al.* [2002] at midlatitudes and from ground-based and space-based measurements by *Steinbrecht et al.* [2006] and *Nair et al.* [2013] for the midlatitude lidar stations, with the trends being around $-0.75 \pm 0.12\%$ yr^{-1}.

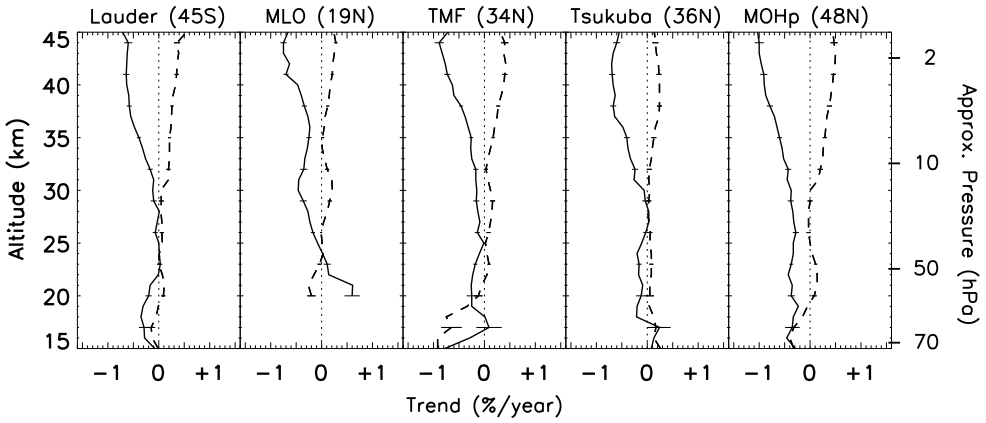

Figure 4. The year-round ozone trends estimated using PWLT functions from the average ozone anomalies computed from the station-based data sets over 1985–1997 (solid lines; MLO trends are for the period 1985–1995) and 1997–2012 (dashed lines; MLO trends are for the period 1995–2012) with 2 sigma errors. The dotted lines represent 0% yr^{-1}.

Table 1. The Year-Round Ozone Trends Along With Their 2 Sigma Error in % yr^{-1} Estimated Using PWLT Functions for the Northern Midlatitudes (Average of Ozone Anomalies Over MOHp, Tsukuba, and TMF) Compared to the Trends Calculated Using the Combined SAGE II and GOMOS Ozone Data for Northern Midlatitudes by *Kyrölä et al.*[2013][a]

Altitude Range (km)	Trend (% yr^{-1}) *Kyrölä et al.* [2013]	Trend (% yr^{-1}) This Study
	1984–1997	1985–1997
20–25	**−0.2**	**−0.3 ± 0.07**
25–35	**−1.6**	**−0.35 ± 0.06**
35–45	**−0.7**	**−0.7 ± 0.06**
	1997–2011	1997–2012
20–25	−0.25	−0.25±0.15
25–35	−0.17	+0.05±0.06
35–45	**+0.15**	**+0.28 ± 0.06**

[a]The trends shown for *Kyrölä et al.* [2013] are extracted from their Figures 14 and 15, and therefore, the errors are not mentioned. The significant trend values are shown in bold.

4.2. Trends During 1997–2012

The dashed lines in Figure 4 represent ozone trends derived from the station-based data sets over 1997–2012 (1995–2012 for MLO). At Lauder, TMF, Tsukuba, and MOHp positive trends of about 0.2 ± 0.06 to 0.5 ± 0.06% yr^{-1} are observed at 35–45 km and are statistically significantly different from zero at the 95% confidence interval. The trends (0.1 ± 0.05% yr^{-1}) at 26–31 km at TMF and those (0.1 ± 0.03% yr^{-1}) at 20–24 km over MOHp are also statistically significant. However, the trends at 23–30 km were neither significant nor negative during the halogen loading phase too at Lauder and Tsukuba, as discussed previously [see also *WMO*, 2011]. Below 20 km, the PWLT trends are negative except at Tsukuba where insignificant positive trends are estimated. At MLO, trends vary from +0.15 ± 0.06 to +0.3 ± 0.04% yr^{-1} above 26 km and are statistically significant, too, except around 35 km, while trends are found to be negative below 25 km (−0.3 ± 0.1% yr^{-1}). The negative trends estimated in the subtropical lower stratosphere (e.g., MLO) can also be seen in the studies of *Gebhardt et al.* [2014] and *Kyrölä et al.* [2013].

As presented in Table 1, we find a statistically significant but slightly larger trend of about +0.28 ± 0.06% yr^{-1} at 35–45 km than that found by *Kyrölä et al.* [2013] (extracted from their Figure 15) at northern midlatitudes in 1997–2012. Our analysis at 25–35 km in the northern midlatitude shows insignificant trend of about +0.05±0.06% yr^{-1}, although *Kyrölä et al.* [2013] derive a trend of −0.17% yr^{-1} there, which was also statistically insignificant. *Jones et al.* [2009] find insignificant positive trends (0.2 ± 1.9% yr^{-1} at 20–25 km, 0.8 ± 1.5% yr^{-1} at 25–35 km, and 1.4 ± 2.3% yr^{-1} at 35–45 km) for the 1997–2008 period. The slight difference with our trend estimates here can be due to the difference in the length of the analysis periods, as our estimates include four additional years. The trend found in the northern lower stratosphere is about −0.25 ± 0.15% yr^{-1} and is statistically significantly different from zero at the 95% confidence interval. A similar trend is also found in the study of *Kyrölä et al.* [2013] in the lower stratosphere, as compiled in Table 1. Differences in various trend estimates could be due to the differences in data sets, proxy data, and the period of trend analyses. These results imply that the ozone recovery signal is very obvious in the upper stratosphere. In the lower and middle stratosphere, ozone recovery is evading detection due to the large variability in the dynamics over recent years, as explained in section 4.

4.3. On the Trends of Individual Measurements

As emphasized earlier, the motivation for combining different ground-based and space-based data sets was to make a debiased long-term data set suitable for ozone trend studies, as performed in this study and discussed previously by others [e.g., *Steinbrecht et al.*, 2009; *Jones et al.*, 2009; *Nair et al.*, 2013; *Kyrölä et al.*, 2013]. Individual trend analysis using each satellite- and ground-based measurement at each station is beyond the scope of this study. In addition, since the individual instruments have different observation periods (e.g., SAGE II: 1985–2005 and HALOE: 1991–2005) and independent instrumental drifts, meaningful long-term trend calculations and their comparisons are hardly possible, in particular for the post-1997 ozone recovery

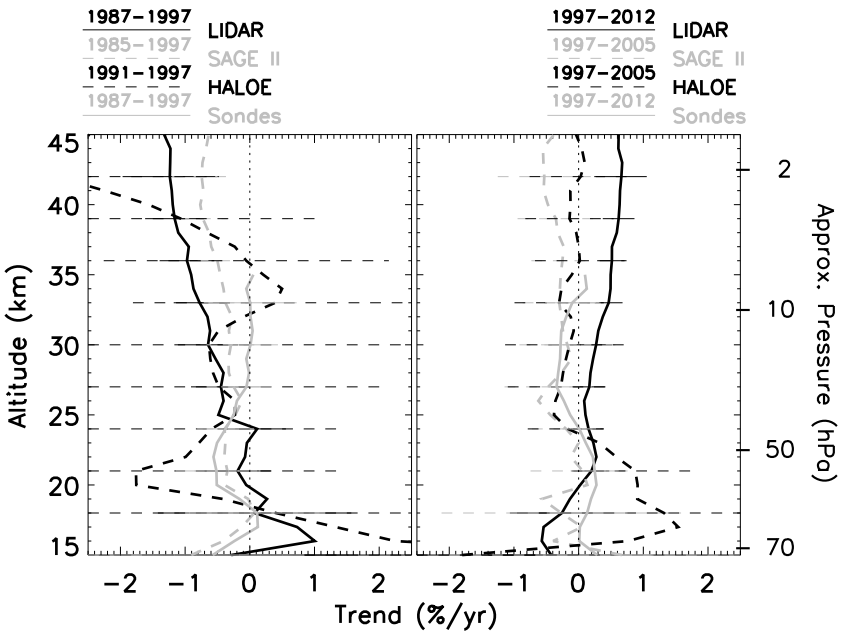

Figure 5. The year-round ozone trends estimated using PWLT functions from the individual ozone anomalies at MOHp (48°N) with 2 sigma errors. The *Sondes* represent the ozonesonde measurements. The dotted lines represent 0% yr^{-1}.

analysis period. For instance, Figure 5 shows ozone trends estimated from the HALOE, SAGE II, ozonesondes, and lidar measurements for the pre-1997 and post-1997 periods at MOHp. As expected, the long-term data (e.g., lidar) yield similar vertical distribution and comparable trend values to those found from the average ozone anomaly for both periods, such as around $-0.5 \pm 0.3\%$ yr^{-1} at 26–35 km and around $-1.2 \pm 1.0\%$ yr^{-1} at 40–45 km for the pre-1997 period and $+0.5 \pm 0.3\%$ yr^{-1} above 35 km for the post-1997 period. In contrast, the short-term data show different and insignificant trends (e.g., HALOE trends: $-2.15 \pm 2.5\%$ yr^{-1} at 40–41 km in 1991–1997 and $-0.15 \pm 0.75\%$ yr^{-1} at 40–45 km in 1997–2005). These results suggest that the comparison of trends derived from the individual measurements over different periods is not viable to draw strong conclusions. Note also that the trends computed by the PWLT method depend on the length of the data record. Nevertheless, it is worth mentioning that the trends derived from the long-term lidar data are comparable to those calculated by *Steinbrecht et al.* [2006] for MOHp (about $-0.58 \pm 0.08\%$ yr^{-1}) and by *Jones et al.* [2009] for 30–60°N (about $-0.72 \pm 0.09\%$ yr^{-1}) in the upper stratosphere for the pre-EESC peak period.

4.4. Sensitivity of the Derived Ozone Trends

To check the robustness of the trends found over individual sites, trends are also computed from the GOZCARDS merged satellite ozone data [*Froidevaux et al.*, 2015], as done by *Nair et al.* [2013]. As GOZCARDS data are also made from similar satellite data sets as those used over the stations, the analysis using GOZCARDS zonal mean data would be a good tool for comparing the trends over the stations. The regression is done on ozone anomalies in latitude bands of 20–30°, 30–40°, 40–50°, 50–60°, and 30–60° for both hemispheres. The monthly ozone anomalies in percent are calculated from ozone VMRs, as mentioned for the station-based data sets in the previous sections. The resulting PWLT estimates on pressure grids for the 1979–1997 and 1997–2012 (1979–1995 and 1995–2012 for subtropics) periods are shown in Figure 6.

In 1979–1997 (1979–1995 for subtropics), significant trends of -0.3 ± 0.08 to $-0.7 \pm 0.07\%$ yr^{-1} are estimated in the upper stratosphere (5–1 hPa) at all latitude bands. The trends are very small or insignificant at 31–10 hPa in the midlatitudes, consistent with the results observed for the station-based analyses at 22–30 km. The trends at 40–50° N/S are about -0.3 ± 0.09 to $-0.8 \pm 0.08\%$ yr^{-1} at 5–2 hPa and are comparable to the trends estimated over the stations that fall in these latitude bands: Lauder (45°S) and MOHp (48°N), with trends ranging from -0.3 ± 0.08 to $-0.9 \pm 0.07\%$ yr^{-1} at 35–45 km. Similarly, trends found at 20–30°N (-0.2 ± 0.08 to $-0.6 \pm 0.07\%$ yr^{-1}) show matching values to those computed over MLO (19°N), and trends found over 30–40°N are in very good agreement with those estimated at TMF (34°N) and Tsukuba (36°N) in the upper stratosphere, with trends of -0.4 ± 0.08 to $0.6 \pm 0.07\%$ yr^{-1}.

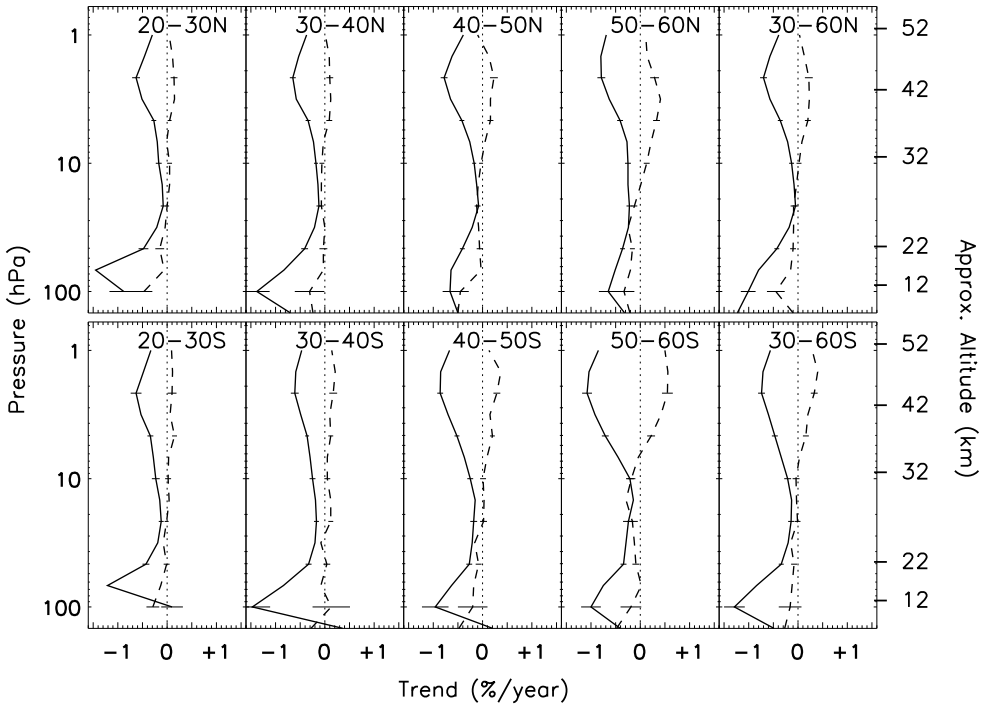

Figure 6. The year-round ozone trends estimated using PWLT functions from the GOZCARDS ozone anomaly data at different latitude bands over 1979–1997 (solid lines; the subtropical trends are for the period 1979–1995) and 1997–2012 (dashed lines; the subtropical trends are for the period 1995–2012) with 2 sigma errors. The dotted lines represent 0% yr^{-1}.

In 1997–2012 (1995–2012 for subtropics), the analysis of upper stratospheric GOZCARDS data shows significant positive trends of about 0.3 ± 0.08% yr^{-1} at midlatitudes and 0.2 ± 0.08% yr^{-1} in the subtropics (for 5–2 hPa or ~35–45 km), which are also in agreement with the trends estimated over the lidar sites; e.g., the trends (+0.2 ± 0.09% yr^{-1}) estimated at 40–50°S are comparable to those found at Lauder at ~35–45 km. The trends (+0.1 ± 0.09 to +0.4 ± 0.08% yr^{-1}) found over 30–40°N in the upper stratosphere are in good agreement with the trends found over TMF and Tsukuba at 35–45 km. The trends are nearly zero or negative below 4.6 hPa in the midlatitudes and below 21.5 hPa in the subtropics. In short, the regression analysis for the post-EESC peak period shows that the ozone has started to recover in the upper stratosphere but suggests that the dynamical changes have a great impact in slowing down, or masking, the recovery of lower stratospheric ozone, as discussed for the lidar sites in section 4.2.

The GOZCARDS ozone trends are relatively larger in the lower stratosphere over 1979–1997 (1979–1995 for subtropics), but the exact reasons for this are not known yet. However, any trend/bias in the temperature data used to make a common vertical coordinate for the merged data set can impact the ozone trends. Although not that pronounced in the station-based data, the upper stratospheric (5–1 hPa) GOZCARDS ozone trends in the Southern Hemisphere are slightly larger than in the Northern Hemisphere after the EESC peak year. Since the dynamical activity is comparatively lower in the Southern Hemisphere, the estimated trends are more obvious there. Note that the diurnal variation in ozone can be up to 10% in the upper stratosphere [*Parrish et al.*, 2014]. Differences in upper stratospheric ozone trends between GOZCARDS and station-based data may be partly tied to diurnal effects in the various measurements. While the data over lidar sites do not use any special approach, the GOZCARDS methodology adjusts the satellite monthly zonal mean data sets to the average of sunrise and sunset monthly values from SAGE II. Also, the GOZCARDS data spatial average (latitude band of 10°) is comparatively larger than that of the station-based data. The slight differences between the trend values estimated from the station-based and GOZCARDS data are also likely caused (in part) by the extent of GOZCARDS data to 1979 compared to the starting year 1985 for the former data, as the trend estimates are sensitive to the length of the data records; this is also demonstrated by the individual trend analyses shown in Figure 5. Apart from that, the results over the lidar sites and from the GOZCARDS are on different vertical coordinates, although this does not raise a major concern as far as the recovery is concerned, as mentioned in

Nair et al. [2013]. Nevertheless, the aforementioned points are to be recalled when comparing ozone trends from station-based and merged satellite-based data sets.

5. Conclusions

We have used the PWLT regression method to quantify trends in stratospheric ozone from the observations over different lidar sites and a merged satellite data record, GOZCARDS, in the midlatitudes and subtropics. During the halogen loading phase, prior to 1997, negative trends are found throughout the stratosphere, confirming the findings of previous studies on midlatitude ozone trends in the stratosphere [*Kyrölä et al.*, 2013; *Kirgis et al.*, 2013; *Nair et al.*, 2013; *Steinbrecht et al.*, 2006; *WMO*, 2011]. In 1997–2012, both satellite- and ground-based analyses reveal significant positive trends of $0.2 \pm 0.08\%\ yr^{-1}$ to $0.5 \pm 0.07\%\ yr^{-1}$ at midlatitudes and $0.2 \pm 0.08\%\ yr^{-1}$ to $0.3 \pm 0.07\%\ yr^{-1}$ at subtropical latitudes in the upper stratosphere (35–45 km). Thus, clear ozone recovery signals are found in the midlatitudes and subtropical upper stratosphere. Nonetheless, no recovery sign could be detected in the lower stratosphere (15–25 km) mainly due to the large interannual variations in meteorology and dynamics, such as the planetary wave activity, QBO, and ENSO during the recent years. This implies that the ozone recovery in the lower stratosphere is more tied to the variations in meteorology rather than the abundances of halogens at present, although there is a reduction in the levels of stratospheric halogens [*Kohlhepp et al.*, 2012; *Jones et al.*, 2011; *Mäder et al.*, 2010; *Froidevaux et al.*, 2006] due to their production ban by the Montreal Protocol [*WMO*, 2011].

Acknowledgments
The ground-based lidar and ozonesonde data were obtained from the publicly available NDACC (http://www.ndacc.org) and WOUDC (http://www.woudc.org). Measurements at NIWA Lauder are core funded through New Zealands Ministry of Business, Innovation and Employment. The satellite data HALOE are from http://haloe.gats-inc.com/download/index.php, SAGE II from https://eosweb.larc.nasa.gov/, and MLS from http://disc.sci.gsfc.nasa.gov/services. We thank the National Aeronautics and Space Administration (NASA) Langley Research Center (LaRC) and the NASA Langley Chemistry and Dynamics Branch for providing SAGE II data, the collaborative institutes of the NASA-LaRC for maintaining HALOE data, and the NASA Goddard Earth Sciences Data and Information Services Center (GES DISC) for the MLS data. The GOZCARDS data used in this effort were acquired as part of the activities of NASA's Science Mission Directorate and are archived and distributed by the GES DISC at http://disc.sci.gsfc.nasa.gov. All the proxy data (QBO, ENSO, Aerosol, and Solar Flux) used for the regression analysis are available online, and the data sources are given in the text itself (section 3). We thank H. Nakane, National Institute for Environmental Studies, Ibaraki, Japan, and T. Uekubo, Japan Meteorological Agency, Japan, for providing the lidar and ozonesonde data, respectively. A part of this work was performed during P.J.N.'s tenure at CESS Thiruvananthapuram, and hence, the affiliation of that institute is given there. P.J.N. thanks N.P. Kurian, the director of CESS, and V. Nandakumar for their help. We thank E. Kyrölä of FMI, Finland, for his help with providing the trend values from their study. Work at the Jet Propulsion Laboratory, California Institute of Technology was done under contract with the NASA.

References

Cunnold, D. M., E.-S. Yang, M. J. Newchurch, G. C. Reinsel, J. M. Zawodny, and J. M. Russell III (2004), Comment on "Enhanced upper stratospheric ozone: Sign of recovery or solar cycle effect?" by W. Steinbrecht et al., *J. Geophys. Res.*, *109*, D14305, doi:10.1029/2004JD004826.

Damadeo, R. P., J. M. Zawodny, L. W. Thomason, and N. Iyer (2013), SAGE version 7.0 algorithm: Application to SAGE II, *Atmos. Meas. Tech.*, *6*, 3539–3561, doi:10.5194/amt-6-3539-2013.

Damadeo, R. P., J. M. Zawodny, and L. W. Thomason (2014), Reevaluation of stratospheric ozone trends from SAGE II data using a simultaneous temporal and spatial analysis, *Atmos. Chem. Phys.*, *14*, 13,455–13,470, doi:10.5194/acp-14-13455-2014.

Froidevaux, L., et al. (2006), Temporal decrease in upper atmospheric chlorine, *Geophys. Res. Lett.*, *33*, L23812, doi:10.1029/2006GL027600.

Froidevaux, L., et al. (2015), Global OZone Chemistry and Related Datasets for the Stratosphere (GOZCARDS): Methodology and sample results with a focus on HCl, H_2O, and O_3, *Atmos. Chem. Phys. Discuss.*, *15*, 5849–5947, doi:10.5194/acpd-15-5849-2015.

Gebhardt, C., A. Rozanov, R. Hommel, M. Weber, H. Bovensmann, J. P. Burrows, D. Degenstein, L. Froidevaux, and A. M. Thompson (2014), Stratospheric ozone trends and variability as seen by SCIAMACHY from 2002 to 2012, *Atmos. Chem. Phys.*, *14*, 831–846, doi:10.5194/acp-14-831-2014.

Jones, A., et al. (2009), Evolution of stratospheric ozone and water vapour time series studied with satellite measurements, *Atmos. Chem. Phys.*, *9*, 6055–6075, doi:10.5194/acp-9-6055-2009.

Jones, A., J. Urban, D. P. Murtagh, C. Sanchez, K. A. Walker, N. J. Livesey, L. Froidevaux, and M. L. Santee (2011), Analysis of HCl and ClO time series in the upper stratosphere using satellite data sets, *Atmos. Chem. Phys.*, *11*, 5321–5333, doi:10.5194/acp-11-5321-2011.

Kirgis, G., T. Leblanc, I. S. McDermid, and T. D. Walsh (2013), Stratospheric ozone interannual variability (1995–2011) as observed by lidar and satellite at Mauna Loa Observatory, HI and Table Mountain Facility, CA, *Atmos. Chem. Phys.*, *13*, 5033–5047, doi:10.5194/acp-13-5033-2013.

Kohlhepp, R., et al. (2012), Observed and simulated time evolution of HCl, $ClONO_2$, and HF total column abundances, *Atmos. Chem. Phys.*, *12*, 3527–3556, doi:10.5194/acp-12-3527-2012.

Kuttippurath, J., and G. Nikulin (2012), A comparative study of the major sudden stratospheric warmings in the Arctic winters 2003/2004–2009/2010, *Atmos. Chem. Phys.*, *12*, 8115–8129, doi:10.5194/acp-12-8115-2012.

Kuttippurath, J., F. Lefèvre, J.-P. Pommereau, H. K. Roscoe, F. Goutail, A. Pazmiño, and J. D. Shanklin (2013), Antarctic ozone loss in 1979–2010: First sign of ozone recovery, *Atmos. Chem. Phys.*, *13*, 1625–1635, doi:10.5194/acp-13-1625-2013.

Kyrölä, E., M. Laine, V. Sofieva, J. Tamminen, S.-M. Päivärinta, S. Tukiainen, J. Zawodny, and L. Thomason (2013), Combined SAGE II GOMOS ozone profile data set for 1984–2011 and trend analysis of the vertical distribution of ozone, *Atmos. Chem. Phys.*, *13*, 10,645–10,658, doi:10.5194/acp-13-10645-2013.

Livesey, N. J., W. G. Read, L. Froidevaux, J. W. Waters, M. L. Santee, H. C. Pumphrey, D. L. Wu, Z. Shippony, and R. F. Jarnot (2011), *Earth Observing System (EOS) Aura Microwave Limb Sounder (MLS) Version 3.3 Level 2 Data Quality and Description Document, PL D-33509*, Jet Propul. Lab., Calif. Inst. of Technol., Pasadena, Calif., 91109-8099.

Long, C., and J. R. Christy (2012), [Global climate] Lower stratospheric temperature [in State of the Climate in 2011], *Bull. Am. Meteorol. Soc.*, *93*(7), S16–S18.

Mäder, J. A., J. Staehelin, T. Peter, D. Brunner, H. E. Rieder, and W. A. Stahel (2010), Evidence for the effectiveness of the Montreal Protocol to protect the ozone layer, *Atmos. Chem. Phys.*, *10*, 12,161–12,171.

Nair, P. J., et al. (2012), Relative drifts and stability of satellite and ground-based stratospheric ozone profiles at NDACC lidar stations, *Atmos. Meas. Tech.*, *5*, 1301–1318, doi:10.5194/amt-5-1301-2012.

Nair, P. J., et al. (2013), Ozone trends derived from the total column and vertical profiles at a northern mid-latitude station, *Atmos. Chem. Phys.*, *13*, 10,373–10,384, doi:10.5194/acp-13-10373-2013.

Newman, P. A., J. S. Daniel, D. W. Waugh, and E. R. Nash (2007), A new formulation of equivalent effective stratospheric chlorine (EESC), *Atmos. Chem. Phys.*, *7*, 4537–4552, doi:10.5194/acp-7-4537-2007.

Parrish, A., et al. (2014), Diurnal variations of stratospheric ozone measured by ground-based microwave remote sensing at the Mauna Loa NDACC site: Measurement validation and GEOSCCM model comparison, *Atmos. Chem. Phys.*, *14*, 7255–7272, doi:10.5194/acp-14-7255-2014.

Press, W. H., B. P. Flannery, S. A. Teukolsky, and W. T. Vetterling (Eds.) (1989), *Numerical Recipes*, pp. 504–508, Cambridge Univ. Press, Cambridge, U. K.

Reinsel, G. C., E. C. Weatherhead, G. C. Tiao, A. J. Miller, R. M. Nagatani, D. J. Wuebbles, and L. E. Flynn (2002), On detection of turnaround and recovery in trend for ozone, *J. Geophys. Res.*, *107*(D10), 4078, doi:10.1029/2001JD000500.

Russell, J. M., L. L. Gordley, J. H. Park, S. R. Drayson, W. D. Hesketh, R. J. Cicerone, A. F. Tuck, J. E. Frederick, J. E. Harries, and P. J. Crutzen (1993), The halogen occultation experiment, *J. Geophys. Res.*, *98*, 10,777–10,797.

Steinbrecht, W., et al. (2006), Long-term evolution of upper stratospheric ozone at selected stations of the Network for the Detection of Stratospheric Change (NDSC), *J. Geophys. Res.*, *111*, D10308, doi:10.1029/2005JD006454.

Steinbrecht, W., et al. (2009), Ozone and temperature trends in the upper stratosphere at five stations of the Network for the Detection of Atmospheric Composition Change, *Int. J. Remote Sens.*, *30*, 3875–3886, doi:10.1080/01431160902821841.

Steinbrecht, W., U. Köhler, H. Claude, M. Weber, J. P. Burrows, and R. J. van der A (2011), Very high ozone columns at northern mid-latitudes in 2010, *Geophys. Res. Lett.*, *38*, L06803, doi:10.1029/2010GL046634.

Wang, H. J., D. M. Cunnold, L. W. Thomason, J. M. Zawodny, and G. E. Bodeker (2002), Assessment of SAGE version 6.1 ozone data quality, *J. Geophys. Res.*, *107*(D23), 4691, doi:10.1029/2002JD002418.

Wang, R., L. Froidevaux, J. Anderson, R. A. Fuller, P. F. Bernath, M. P. McCormick, N. J. Livesey, J. M. Russell III, K. A. Walker, and J. M. Zawodny (2013), *GOZCARDS Merged Data for Ozone Monthly Zonal Means on a Geodetic Latitude and Pressure Grid, Version 1.01*, NASA Goddard Earth Science Data and Information Services Center, Greenbelt, MD, Accessed 02 May, doi:10.5067/MEASURES/GOZCARDS/DATA3006.

Wohltmann, I., R. Lehmann, M. Rex, D. Brunner, and J. A. Mäder (2007), A process-oriented regression model for column ozone, *J. Geophys. Res.*, *112*, D12304, doi:10.1029/2006JD007573.

World Meteorological Organization (WMO) (2011), Scientific Assessment of Ozone Depletion: 2010, Global Ozone Research and Monitoring Project. Rep. 52, 516 pp., Geneva, Switzerland.

World Meteorological Organization (WMO) (2014), Scientific Assessment of Ozone Depletion: 2014, Global Ozone Research and Monitoring Project. Rep. 55, 416 pp., Geneva, Switzerland.